# Global patterns of land-atmosphere fluxes of carbon dioxide, latent heat, and sensible heat derived from eddy covariance, satellite, and meteorological observations

Martin Jung,[1] Markus Reichstein,[1] Hank A. Margolis,[2] Alessandro Cescatti,[3] Andrew D. Richardson,[4] M. Altaf Arain,[5] Almut Arneth,[6,7] Christian Bernhofer,[8] Damien Bonal,[9] Jiquan Chen,[10] Damiano Gianelle,[11] Nadine Gobron,[12] Gerald Kiely,[13] Werner Kutsch,[14] Gitta Lasslop,[1] Beverly E. Law,[15] Anders Lindroth,[6] Lutz Merbold,[16] Leonardo Montagnani,[17,18] Eddy J. Moors,[19] Dario Papale,[20] Matteo Sottocornola,[11] Francesco Vaccari,[21] and Christopher Williams[22]

Received 30 September 2010; revised 18 May 2011; accepted 6 June 2011; published 3 September 2011.

[1] We upscaled FLUXNET observations of carbon dioxide, water, and energy fluxes to the global scale using the machine learning technique, model tree ensembles (MTE). We trained MTE to predict site-level gross primary productivity (GPP), terrestrial ecosystem respiration (TER), net ecosystem exchange (NEE), latent energy (LE), and sensible heat (H) based on remote sensing indices, climate and meteorological data, and information on land use. We applied the trained MTEs to generate global flux fields at a 0.5° × 0.5° spatial resolution and a monthly temporal resolution from 1982 to 2008. Cross-validation analyses revealed good performance of MTE in predicting among-site flux variability with modeling efficiencies (MEf) between 0.64 and 0.84, except for NEE (MEf = 0.32). Performance was also good for predicting seasonal patterns (MEf between 0.84 and 0.89, except for NEE (0.64)). By comparison, predictions of monthly anomalies were not as strong (MEf between 0.29 and 0.52). Improved accounting of disturbance and lagged environmental effects, along with improved characterization of errors in the training data set, would contribute most to further reducing uncertainties. Our global estimates of LE (158 ± 7 J × $10^{18}$ $yr^{-1}$), H (164 ± 15 J × $10^{18}$ $yr^{-1}$), and GPP (119 ± 6 Pg C $yr^{-1}$) were similar to independent estimates. Our global TER estimate (96 ± 6 Pg C $yr^{-1}$) was likely underestimated by 5–10%. Hot spot regions of interannual variability in carbon fluxes occurred in semiarid to semihumid regions and were controlled by moisture supply. Overall, GPP was more important to interannual variability in NEE than TER. Our empirically derived fluxes may be used for calibration and evaluation of land surface process models and for exploratory and diagnostic assessments of the biosphere.

[1]Model Data Integration Group, Max Planck Institute for Biogeochemistry, Jena, Germany.
[2]Centre d'Étude de la Forêt, Faculté de Foresterie, de Géographie et de Géomatique, Université Laval, Québec, Québec, Canada.
[3]Climate Change and Air Quality Unit, Institute for Environment and Sustainability, Joint Research Centre, European Commission, Ispra, Italy.
[4]Department of Organismic and Evolutionary Biology, Harvard University, Cambridge, Massachusetts, USA.
[5]School of Geography and Earth Sciences and McMaster Centre for Climate Change, McMaster University, Hamilton, Ontario, Canada.
[6]Division of Physical Geography and Ecosystem Analysis, Department of Earth and Ecosystem Sciences, Lund University, Lund, Sweden.
[7]Institute for Meteorology and Climate Research, Atmospheric Environmental Research, Karlsruhe Institute for Technology, Garmisch Partenkirchen, Germany.
[8]Department of Meteorology, Institute of Hydrology and Meteorology, Technische Universität, Dresden, Germany.
[9]INRA, UMR INRA-UHP 1137 Ecologie et Ecophysiologie Forestière, Champenoux, France.
[10]Department of Environmental Sciences, University of Toledo, Toledo, Ohio, USA.
[11]Environment and Natural Resources Area, Research and Innovation Centre, IASMA, Fondazione Edmund Mach, Trento, Italy.
[12]Global Environmental Monitoring Unit, Institute for Environment and Sustainability, European Commission Joint Research Centre, Ispra, Italy.
[13]HYDROMET, Civil and Environmental Engineering Department, University College Cork, Cork, Ireland.
[14]Institut für Agrarrelevante Klimaforschung, Johann Heinrich von Thünen-Institut, Braunschweig, Germany.
[15]Department of Forest Ecosystems and Society, Oregon State University, Corvallis, Oregon, USA.
[16]Grassland Science Group, Institute of Plant-, Animal- and Agroecosystem Sciences, ETH Zurich, Zurich, Switzerland.
[17]Forest Services and Agency for the Environment, Autonomous Province of Bolzano, Bolzano, Italy.
[18]Faculty of Science and Technology, Free University of Bolzano, Bolzano, Italy.
[19]Earth System Science and Climate Change, Alterra Wageningen UR, Wageningen University, Wageningen, Netherlands.
[20]Department of Forest Environment and Resources, University of Tuscia, Viterbo, Italy.
[21]Institute of Biometeorology, National Research Council, Firenze, Italy.
[22]Graduate School of Geography, Clark University, Worcester, Massachusetts, USA.


0148-0227/11/2010JG001566

**Citation:** Jung, M., et al. (2011), Global patterns of land-atmosphere fluxes of carbon dioxide, latent heat, and sensible heat derived from eddy covariance, satellite, and meteorological observations, *J. Geophys. Res.*, *116*, G00J07, doi:10.1029/2010JG001566.

## 1. Introduction

[2] The exchanges of carbon, water, and energy between the terrestrial biosphere and the atmosphere are major drivers of the Earth's climate system. At the ecosystem scale, the net exchanges of carbon dioxide, water and energy between the land surface and the atmosphere are widely measured using the eddy covariance technique. The establishment of a global network of eddy covariance flux towers [*Baldocchi*, 2008; *Baldocchi et al.*, 2001], in conjunction with the availability of global satellite remote sensing and gridded meteorological data sets, now allows us to generate empirical global estimates of key biospheric variables based on observations. This approach is an important step forward because until now, only process-based land surface models (LSMs) have been used to assess variations of carbon and water fluxes at the global scale. However, LSMs are based on theories and hypotheses about biosphere functioning where several partly mechanistic, partly empirical submodels (e.g., photosynthesis, phenology, canopy conductance, respiration) are linked to mimic the behavior of ecosystem carbon, water, and energy fluxes. LSMs have a prescribed and fixed model structure with simplified representation of selected processes and ecosystem components. Hence, LSM simulations may be regarded as the anticipated or hypothesized behavior of the biosphere in response to climate variability or other factors. Substantial disagreements among different LSMs remain for simulations of both present-day [e.g., *Jung et al.*, 2007b; *Weber et al.*, 2009] and future scenarios [e.g., *Friedlingstein et al.*, 2006].

[3] There have been increasing efforts directed at model data fusions such as the optimization of certain model parameters using observations [*Williams et al.*, 2009]. Eddy covariance time series of single sites have been assimilated into LSMs [*Braswell et al.*, 2005; *Spadavecchia et al.*, 2011; *Williams et al.*, 2009]. However, if model structure is not adequate, the model may not fit the observations well, and optimized parameters may be biased [*Carvalhais et al.*, 2008]. Furthermore, even when both eddy covariance data and measurements of other carbon pools and fluxes are used as constraints [e.g., *Richardson et al.*, 2010], substantial uncertainties may remain in model predictions, because the information content of the data may be inadequate to distinguish among competing representations of processes occurring in the model.

[4] In this paper, we explore a data-oriented approach that complements process-oriented modeling approaches. Machine learning algorithms (e.g., artificial neural networks, support vector machines, regression and model trees) construct an empirical model based on the patterns contained in data and are very data adaptive because no functional forms need to be prescribed. Such methods have been applied to the upscaling of eddy covariance measurements from local to continental [e.g., *Papale and Valentini*, 2003; *Xiao et al.*, 2008; *Yang et al.*, 2007], and to some extent, to global scales [*Beer et al.*, 2010; *Jung et al.*, 2010] using remote sensing, meteorological, and land cover data.

[5] MTEs have been used to predict global fields of land surface-atmosphere fluxes from FLUXNET eddy covariance sites using monthly simulations of GPP from a biosphere model from 1998 to 2005 as a synthetic test case [*Jung et al.*, 2009]. In that study, the MTE was trained to predict the simulations of the biosphere model LPJmL [*Bondeau et al.*, 2007] for locations and months with available quality-filtered flux data. Subsequently, the trained MTE was applied globally, and compared to global biosphere model simulations. With a modeling efficiency [*Nash and Sutcliffe*, 1970] of 92%, MTE exhibited excellent performance in reproducing the original simulations of LPJmL.

[6] Here, we use estimates of the fraction of absorbed photosynthetic active radiation (fAPAR) derived from remote sensing, as well as climate and land cover data, to generate global estimates of five important land–atmosphere fluxes: gross primary productivity (GPP), terrestrial ecosystem respiration (TER), net ecosystem exchange (NEE), latent heat (LE), and sensible heat (H) over 27 years (1982–2008) at 0.5° × 0.5° spatial and monthly temporal resolution based on the MTE approach. We present a synoptic characterization and exploratory analysis of the spatial and temporal variability and discuss uncertainties and limitations of our data products. Our specific objectives are (1) to assess the capacity of MTE to predict GPP, TER, NEE, LE, and H fluxes using cross validation; (2) to quantify globally integrated mean annual biosphere-atmosphere fluxes, and to assess their spatial patterns; (3) to characterize global spatial patterns of seasonal variability in these fluxes, and (4) to identify and diagnose the drivers of carbon fluxes in regions with large interannual variability (commonly referred to as "hot spot" regions).

## 2. Methods

### 2.1. Overview

[7] Machine learning algorithms construct a model based on data and are typically data limited. This "data limitation" refers to the quantity, quality, and representativeness of the training data set. An important aspect of the data limitation is the availability of relevant explanatory variables, which include both the site-level in situ information and the corresponding global grids. Thus, some otherwise pertinent data must be ignored because either corresponding site information or respective global data sets do not exist or are insufficient. Examples include information on land use history, disturbance history, soil moisture, and fertility. The requirement that all predictor variables are available for all sites and grid cells is a major obstacle to empirical upscaling.

[8] The overall upscaling procedure involves three main steps: (1) processing and quality control of the FLUXNET data, (2) training MTEs for each biosphere-atmosphere flux of interest using site-level explanatory variables and fluxes, and (3) applying the established MTEs for global upscaling, using gridded data sets of the same explanatory variables. We chose a monthly time step for four reasons: (1) noise in

the data sets (particularly in eddy covariance and remote sensing data) is reduced by aggregation; (2) seasonality is preserved and a sufficient number of data points for MTE training are retained, (3) greater computational efficiency is achieved compared to running at a daily time step, and (4) observation based global gridded data products are commonly available and with highest confidence at monthly time steps.

[9] We forced 25 individual model trees for each biosphere-atmosphere flux using gridded inputs from 1982 to 2008. The best estimate of a biosphere-atmosphere flux for further analysis is the median over the 25 estimates for each pixel and month. Uncertainties were estimated by repeating a given calculation (e.g., the global total value) for each of the 25 tree outputs and computing the median absolute deviation (MAD) of the individual model tree outputs and multiplying it by 1.483. This is equivalent to one standard deviation for a normal distribution but is more robust against outliers and assumptions about the distribution. Our uncertainty estimates reflect a structural uncertainty of the model trees, i.e., the mapping of X to Y. *Jung et al.* [2009] inferred that this uncertainty estimate increases in the case of extrapolation to environmental domains, which are not covered by the training data. Other sources of uncertainty such as measurement uncertainties of eddy covariance fluxes [*Lasslop et al.*, 2008; *Richardson et al.*, 2006; *Richardson et al.*, 2008] or uncertainties of global gridded data of explanatory variables [e.g., *Hicke*, 2005; *Zhao et al.*, 2006] are not accounted for in this uncertainty measure.

### 2.2. Model Tree Ensembles

[10] Model trees stratify the data set into a hierarchical order according to decisions such as X1 "greater than" or "less than." The final domains of the tree (leaves) are defined by a series of decisions and we used a multiple linear function to model the target (Y) variable for this domain. The nature of the stratification allows us to approximate any nonlinear relationship even with linear models in the leaves. The model tree ensemble approach (MTE) employed in this paper is based on the TRIAL+ERROR algorithms [*Jung et al.*, 2009]. The model Tree Induction Algorithm (TRIAL) grows a model tree from the root node and finds the split decision at each node by minimizing the sum of squared errors of multiple regressions in both subdomains. To prevent over fitting, the tree growth is stopped when the Schwarz criterion (aka Bayesian Information Criterion, BIC [*Schwarz*, 1978]) increases. The Schwarz criterion is calculated from the mean squared error of the model tree as determined by tenfold cross validation in the leaves, the number of parameters of the model tree, and the number of samples. A stepwise forward selection of regression variables based on the BIC is used to establish the multiple linear regressions in the leaves to reduce the number of parameters and to better constrain regression coefficients in the presence of colinearity. TRIAL is capable of incorporating different kinds of explanatory variables: those that are only used for decisions (split variables); those that are only used in the multiple regressions in the leaves (regression variables); and those which can serve as both, split and regression variables.

[11] Ensembles of model trees were generated by coupling TRIAL to the ERROR (Evolving tRees with RandOm gRowth) algorithm. ERROR first generates a large number of trees by taking an existing tree, removing part of it, letting it grow according to random decisions, and finding the best decisions for the final leaves using TRIAL. Subsequently, a subset of model trees that exhibit best performances (measured by the Schwarz criterion) and are independent from each other (according to the conditions of all leaves), was selected for the ensemble. Details of the MTE approach and a validation are given by *Jung et al.* [2009].

### 2.3. FLUXNET Eddy Covariance Data

[12] Flux measurements are affected by both random and systematic (bias) errors, which arise from limitations of the measurement technique, the stochastic nature of turbulence, and site-specific differences in data processing protocols [e.g., *Moncrieff et al.*, 1996; *Papale et al.*, 2006; *Richardson et al.*, 2006; *Richardson et al.*, 2008]. Substantial efforts were made in harmonizing the processing and quality control of the measurements, and in characterizing their uncertainties. However, a significant remaining problem is the quantification of systematic biases of flux measurements, particularly as related to advection [e.g., *Aubinet*, 2008] and energy balance closure [*Foken*, 2008].

[13] We processed half-hourly FLUXNET eddy covariance measurements using standardized procedures of gap filling and quality control [*Moffat et al.*, 2007; *Papale et al.*, 2006], and the data were subsequently aggregated into monthly means, which diminishes random errors. We excluded data where more than 20% of the data of the monthly mean was based on gap filling with low confidence [*Reichstein et al.*, 2005] to minimize uncertainty originating from gap filling. Estimates of GPP and TER can be derived from the NEE measurements using two independent flux partitioning methods [*Reichstein et al.*, 2005; *Lasslop et al.*, 2010]. *Reichstein et al.* [2005] calculated the temperature sensitivity of respiration using nighttime NEE data and extrapolated those to daytime to estimate TER. In contrast, *Lasslop et al.* [2010] used mainly daytime NEE data to constrain a hyperbolic light response curve for the estimation of GPP, accounting for the temperature response of respiration and effects of vapor pressure deficit (VPD) on photosynthesis. To avoid redundancy, our analysis is based on only one estimate of GPP and TER. We chose GPP based on the work by *Lasslop et al.* [2010] and TER based on the work by *Reichstein et al.* [2005] because they are largely independent estimates.

[14] Because the energy balance at eddy covariance sites is usually not closed, we performed corrections of monthly LE and H measurements according to *Twine et al.* [2000], which preserves the Bowen ratio:

$$F_{corrected} = A \times F_{uncorrected} = (Rn - G)/(H_{uncorrected} + LE_{uncorrected}) \times F_{uncorrected} \quad (1)$$

Here, F is the energy flux (either LE or H), A is the correction factor, Rn is the net radiation, and G the soil heat flux. We estimated A based on a regression between A and A* ($R^2 \sim 0.98$) in cases where G had not been measured:

$$A^* = Rn/(H_{uncorrected} + LE_{uncorrected}) \quad (2)$$

Our approach to correct for the energy balance residual is not universally accepted in the scientific community because

**Table 1.** List of Explanatory Variables Used for the Training of MTEs[a]

| Variable | Type | Type of Variability |
|---|---|---|
| *Climate (for Data Stratification)* | | |
| Mean annual temperature | Split | static |
| Mean Annual precipitation sum | Split | static |
| Mean annual climatic water balance | Split | static |
| Mean annual Potential evaporation | Split | static |
| Mean annual sunshine hours | Split | static |
| Mean annual number of wet days | Split | static |
| Mean annual relative humidity | Split | static |
| Mean monthly temperature | Split | Monthly but static over years |
| Mean monthly precipitation sum | Split | Monthly but static over years |
| Mean monthly climatic water balance | Split | Monthly but static over years |
| Mean monthly potential evaporation | Split | Monthly but static over years |
| Mean monthly sunshine hours | Split | Monthly but static over years |
| Mean monthly number of wet days | Split | Monthly but static over years |
| Mean monthly relative humidity | Split | Monthly but static over years |
| *Vegetation Structure* | | |
| Maximum fAPAR of year | Split | yearly |
| Minimum fAPAR of year | Split | yearly |
| Maximum–minimum fAPAR | Split | yearly |
| Mean annual fAPAR | Split | yearly |
| Sum of fAPAR over the growing season | Split | yearly |
| Mean fAPAR of the growing season | Split | yearly |
| Growing season length derived from fAPAR | Split | yearly |
| Sum of fAPAR × potential radiation of year | Split | yearly |
| Maximum of fAPAR × potential radiation of year | Split and regression | yearly |
| IGBP vegetation type | Split | static |
| *Meteorology* | | |
| Temperature | Split and regression | monthly |
| Precipitation | Split and regression | monthly |
| Potential radiation | Split and regression | Monthly but static over years |
| *Vegetation Status* | | |
| fAPAR | Split and regression | monthly |
| fAPAR × potential radiation | Split and regression | monthly |

[a]Variables that are only split variables are only used for data stratification and do not enter regressions. Please note that not all variables are automatically selected by the model trees. The "type of variability" refers to if and when the values of the respective variable change for a given pixel. "Static" variables never change and can be used by MTE to stratify into spatial domains (e.g., according to long-term mean annual temperature). "Monthly but static over years" refers to mean seasonal cycles, i.e., the values change monthly, but the same monthly values are repeatedly used for all years. "Yearly" variables have the same value within a year, but this value is updated for each year, which is primarily used for variables describing vegetation structure to capture possible effects of land cover change. "Monthly" variables exhibit different values for each month and year; that is, they are continuously updated for each month.

the magnitude and causes of energy balance imbalance likely vary among sites and time scales [e.g., *Barr et al.*, 2006; *Hendricks Franssen et al.*, 2010; *Wilson et al.*, 2002]. However, our approach to correcting measured energy fluxes to force energy balance closure has yielded global LE fluxes that are consistent with independent estimates derived from global precipitation and river runoff data, while no correction yielded systematically low-biased LE estimates [*Jung et al.*, 2010]. Moreover, when the energy balance is closed initially, the correction factor approaches 1 with our method and the measured energy balance fluxes are not changed.

[15] We used a series of consistency checks and filter out uncertain data points in the monthly data set based on a nonparametric outlier test. Data points were removed if they fell outside the range given by the median ±1.5 times the interquartile range. We tested for the consistencies of energy fluxes using the following three criteria: (1) $LE_{uncorrected} + H_{uncorrected} - Rn$, (2) $A - A^*$, (3) $LE_{uncorrected} - A \times LE_{uncorrected}$. For the carbon fluxes, we removed data points that exhibit strong inconsistencies of the two flux partitioning methods using the same outlier test which indicates possible problems due to uncertain nighttime data and therefore possible systematic errors: (1) $GPP_{Reichstein} - GPP_{Lasslop}$, (2) $TER_{Reichstein} - TER_{Lasslop}$, (3) $NEE_{measured} - NEE_{Lasslop}$. In addition, we accounted for uncertainties which originate from determining the u* threshold. The u* uncertainty in the carbon fluxes was inferred by bootstrapping based on the work by *Papale et al.* [2006]. The 5% most uncertain data points of each carbon flux were removed.

### 2.4. Explanatory Variables

[16] We used 29 explanatory variables of four types to train the MTE to predict biosphere-atmosphere fluxes globally (Table 1), including (1) monthly fAPAR from the SeaWiFS sensor, precipitation, and temperature (both in situ measured); (2) annual changes of the fPAR that describe properties of vegetation structure such as minimum, maximum, mean, and amplitude; (3) mean annual climate such as mean annual temperature, precipitation, sunshine hours, relative humidity, potential evapotranspiration, climatic

water balance (precipitation–potential evaporation), and their seasonal dynamics; and (4) the vegetation type according to the IGBP classification plus a flag regarding the photosynthetic pathway (C3, C4, C3/C4) (in situ information). We used only variables of the first category, which vary for each data point in the multiple linear regressions, while the remaining variables were used for data stratification.

[17] The choice of explanatory variables is constrained by the fact that a variable must be available at all sites and must also be available as a global product to be included. In cases where a variable is measured accurately at FLUXNET sites, but corresponding global products of this variable are very uncertain, it may be advantageous to exclude this variable from the analysis, particularly if the variable does not add substantial information to other explanatory variables. We excluded vapor pressure deficit and global radiation as explanatory variables because (1) such global observation based products are lacking and the uncertainty of respective global reanalysis products is high, and (2) gains from inclusion of these two variables were marginal [*Jung et al.*, 2010].

### 2.5. Cross Validation

[18] We evaluated the performance of our approach based on fivefold cross validations. A fivefold cross validation implies that the data set is stratified into five parts with approximately equal number of samples. The target values for each of these five parts are predicted based on the training using the remaining four parts. We conducted two experiments where (1) entire sites were removed from the training (~20%), and (2) consecutive parts of the time series of the sites were removed. Hence, the first cross-validation experiment corresponds to the uncertainty of predicting the flux time series for unknown sites, while the second experiment assesses the uncertainty of filling long gaps in the time series based on the information from all flux sites. The first cross-validation experiment is the most relevant in the context of the objectives of this paper and therefore we discuss mainly these results.

[19] We decomposed the observed and predicted data into three categories of variability: (1) among-site variability, (2) seasonal variation, and (3) anomalies. We first calculated the mean seasonal cycle ($F_{MSC}$) per site, i.e., averaging the values for a month across all available years. We prescribed that at least two values (i.e., years) for a month must be available. To assess the among site variability, we calculated a mean value for each site ($F_{SITE}$) given as the mean of $F_{MSC}$ if at least 6 out of 12 values of $F_{MSC}$ were present. We calculated the seasonal variation $F_{SEAS}$ by removing $F_{SITE}$ from $F_{MSC}$. Anomalies were calculated as the deviation of a flux value from $F_{MSC}$. Finally, we calculated a series of performance measures: Pearson's correlation (Cor), Nash-Sutcliff's modeling efficiency (MEf) [*Nash and Sutcliffe*, 1970], root-mean-square error (RMSE), median absolute deviation (MAD), and ratio of variances (RoV) which is the variance of the predicted values divided by the variance of the observed values. If present, we removed extreme outliers from the computation of performance measures to avoid biased statistics. We identified outliers when data points were outside the range defined by the median of the residuals ±7 times the interquartile range of the residuals.

### 2.6. Global Grids of Explanatory Variables

[20] We constructed a harmonized long-term global fAPAR record from 1982 to 2008 by merging the NDVI product of the Global Inventory Modeling and Mapping Studies (GIMMS) based on the Advanced Very High Resolution Radiometer (AVHRR) [*Tucker et al.*, 2005] with the fAPAR product using Sea-viewing Wide Field-of-view Sensor (SeaWiFS) [*Gobron et al.*, 2006], and the Medium Resolution Imaging Spectrometer (MERIS) [*Gobron et al.*, 2008] at 0.5° × 0.5° spatial resolution. The harmonization procedure of different remote sensing products, covering different periods, adjusts the mean seasonal cycle for each pixel based on the overlapping period (see *Jung et al.* [2010] for details). The final long-term harmonized fAPAR product is based on adjusted GIMMS from 1982 to 1997, SeaWiFS from 1998 to 2005, and adjusted MERIS from 2006 to 2008.

[21] Global upscaling of FLUXNET data over a long time period requires the explanatory variables to be of consistent quality over time, i.e., not containing drifts or other temporal artifacts. We used remote sensing products from older (NDVI from AVHRR from 1982 to 1997) and newer (fAPAR from SeaWiFS and MERIS since 1998) generation sensors. Although the harmonization of the different products was carried out carefully, full consistency cannot be achieved. Continued efforts to reprocess the long-term global AVHRR record should help reduce this source of uncertainty.

[22] Various long-term mean climatic information came from the Climatic Research Unit (CRU) [*New et al.*, 2002] and cover the period 1961–1990. Global grids of monthly precipitation were from GPCC [*Schneider et al.*, 2008]; while global gridded monthly temperature was obtained from a product of the Institute for Climate Impact Research based on CRU data (CRU-PIK) [*Österle et al.*, 2003]. Since neither GPCC or CRU-PIK products were available for 2008, we used the ECMWF ERA interim reanalysis product of *Simmons et al.* [2007] for 2008 after harmonizing ERA-INTERIM with the products for each pixel and month (i.e., adjusting the local mean seasonal cycles). The uncertain quality of global gridded data sets is a universal problem for global modeling activities. Here, we focused on observation-based products (e.g., temperature and precipitation), and avoided the use of more uncertain reanalysis products of vapor pressure deficit and solar radiation.

[23] The global land use data set SYNMAP [*Jung et al.*, 2006] was reclassified into the respective IGBP classes which were used to describe the vegetation at FLUXNET sites from in situ information. We generate fractions of each class globally at 0.5° × 0.5° resolution. Grasslands are further separated into C3, C4, and mixtures of C3/C4 types using the results of [*Winslow et al.*, 2003]; fractions of C3 and C4 crop types were estimated using the gridded database of *Monfreda et al.* [2008], which is based on FAO crop statistics.

[24] Uncertainty of MTE predictions related to uncertain land cover/land use is likely less critical than uncertainty originating from meteorological data. Lessons from an ecosystem modeling exercise over Europe suggested that the sensitivity of the Biome-BGC model to different land cover data sets was much smaller than it was to different climate data forcings, in particular when land cover was aggregated

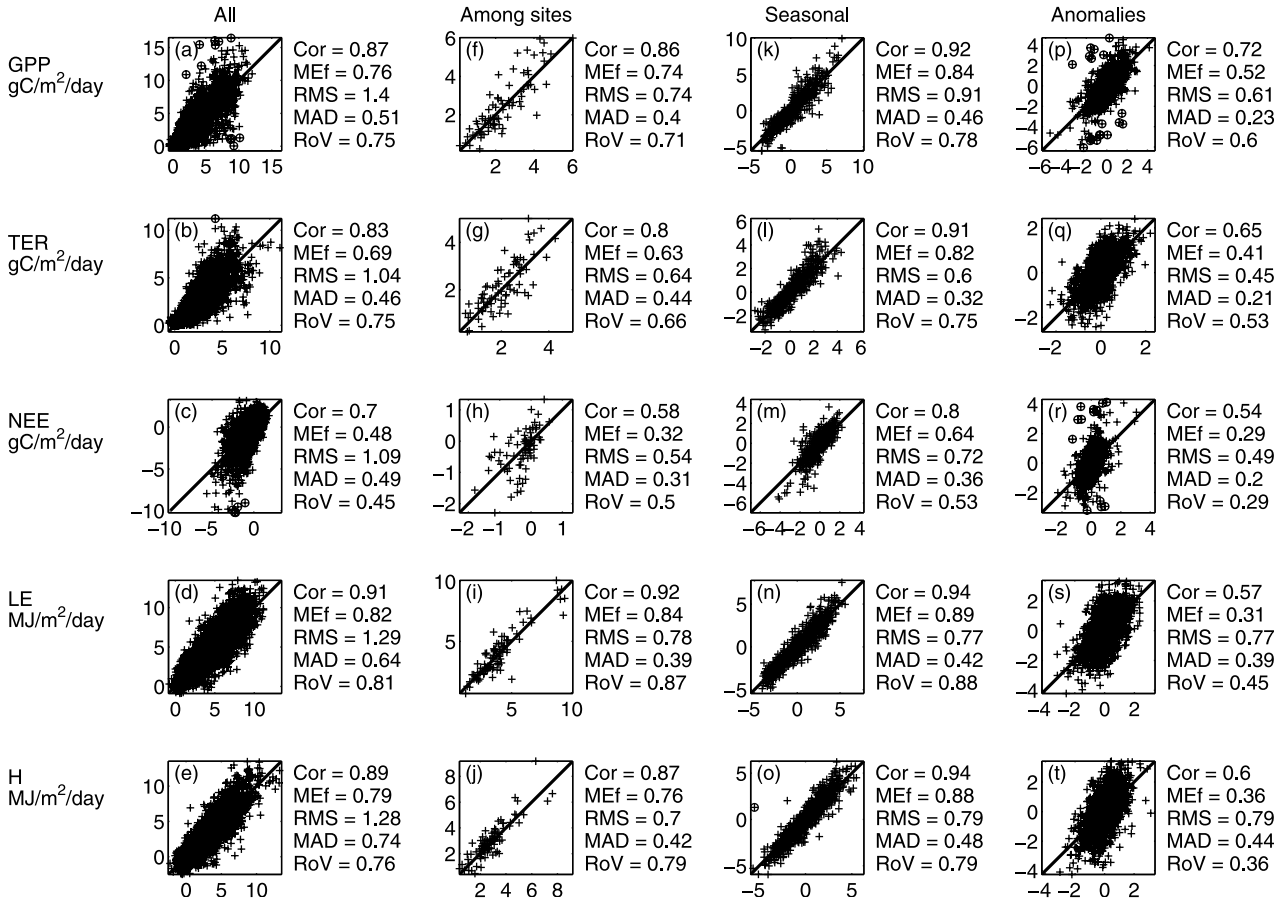


**Figure 1.** MTE predicted (*y* axis) versus FLUXNET observed (*y* axis) GPP, TER, NEE, LE, and H fluxes with performance measures for cross-validation experiment 1 (see section 2.5) for (a–e) all data points, (f–j) among-site variability, (k–o) seasonal variability, and (p–t) anomalies. Outliers are labeled with a circle and were not considered in the calculation of performance measures.

to fractions at coarser resolution [*Jung et al.*, 2007b]. We expect we can transfer this general finding to empirical modeling using MTE. Moreover, the base land cover data set (SYNMAP) used in this paper is already a blend of different remote sensing based land cover data sets which leveraged the agreement among alternative products. However, we used a static land cover map and did not account for land cover change, which introduces uncertainty of modeled interannual variability in regions that experienced extensive land cover/land use conversions over the last decades. Moreover, SYNMAP has no "wetland" class because this class was not consistent with the applied concept of plant functional types.

## 3. Results and Discussion

### 3.1. Performance of MTE Based on Cross Validation

[25] The overall performance of our approach is best for energy fluxes (LE, H) followed by the fluxes of carbon dioxide, i.e., GPP, TER, and NEE (Figure 1). We observe the same pattern for the MTEs' ability to reproduce the among site variability, where LE and H reach modeling efficiency values of 0.84 and 0.76, respectively. Modeling efficiency and RMSE of mean GPP at the site level is 0.74 and 270 g C $m^{-2}$ $yr^{-1}$. For comparison, the RMSE of three ecosystem models (LPJ [*Sitch et al.*, 2003], Orchidee [*Krinner et al.*, 2005], Biome-BGC [*Running and Hunt*, 1993]) for among site variability of GPP of forests in Europe was ~420 g C $m^{-2}$ $yr^{-1}$ [*Jung et al.*, 2007a]. Although the RMSE for the among-site variability of TER (234 g C $m^{-2}$ $yr^{-1}$) is smaller than for GPP, the among-site variation of TER is less well reproduced as measured by the modeling efficiency (0.64) because the variance of among-site TER is smaller. A slightly worse performance for TER is expected because no explicit information on carbon pools and soil conditions was available.

[26] With a modeling efficiency of 0.32 and an RMSE of 197 g C $m^{-2}$ $yr^{-1}$ the among-site variability of NEE is poorly reproduced by MTE, particularly for sites that are strong carbon sinks. Clearly, we are lacking determinants of mean NEE in the predictors for MTE such as soil and biomass pools, disturbances, ecosystem age, management activities and land use history. In general, NEE changes with forest age because of decomposition in early secondary succession, and a decline in net primary production (NPP) in late succession [*Amiro et al.*, 2010]. We used fAPAR in MTE but it does not serve as an adequate proxy for the age effect on NEE because changes in heterotrophic respiration

are not captured by fAPAR (legacy pools and rates), and photosynthetic rates per unit fAPAR and belowground carbon allocation vary with age [*Law and Waring*, 1994]. Mean NEE of croplands is also largely determined by management activities. Accounting for such effects in MTE would require global spatially explicit information on forest age, past disturbances, and management activities, which is unfortunately lacking. Moreover, as conceptually shown by *Piao et al.* [2009], variables that reflect the trends in climate, rather than mean climate, influence NEE and could be considered as additional predictors in the future.

[27] The seasonal variation of carbon and energy fluxes is very well reproduced; MEf values range from 0.82 to 0.89, except for NEE (0.64). The seasonal variation of carbon and energy fluxes is the dominant and also most robust signal in monthly eddy covariance data. We therefore conclude that our empirically derived global patterns of seasonal variations of carbon and energy fluxes can serve as a robust benchmark for global ecosystem models.

[28] Clearly, the anomalies (expressed as the deviation from the mean seasonal cycle) appear to be least well predicted by MTE. MEf values range from 0.29 (NEE) to 0.52 (GPP) and correlations are between 0.54 and 0.72. The variances of predicted anomalies by MTE are only 30 to 60% of the variances of anomalies from FLUXNET data, suggesting an underestimation of the magnitude of anomalies by MTE, which is most evident for NEE. Further analysis has shown that there is a pattern of larger uncertainty for tropical ecosystems and crops (not shown). Several reasons likely contribute to the fact that predicted anomalies appear to be more uncertain: (1) uncertainties in eddy covariance data, (2) uncertainties of explanatory variables, and (3) missing information. The anomalies are a comparatively small signal in the FLUXNET database, which is dominated by the seasonal and among-site variability of fluxes. The signal-to-noise ratio of monthly anomalies of the eddy covariance data is much smaller than for seasonal or among-site variation of fluxes. Uncertainties due to different processing steps such as u* filtering, gap filling, and flux partitioning of NEE into GPP and TER generates some errors in the data which become important when analyzing anomalies. We can also not exclude that our applied correction step for measured LE and H fluxes may modify the anomalies. Thus, not all of the variance in the anomalies of FLUXNET data is "true" information, and very high MEf values are therefore also not expected. However, since we applied various quality filtering criteria to exclude eddy covariance data that are subject to large uncertainty, uncertainty in the remaining eddy covariance data alone cannot explain the mismatch between observed and predicted flux anomalies.

[29] Uncertainties in the explanatory variables play an important role too, and here the most obvious candidates are remotely sensed information such as fAPAR, fAPAR time series for individual pixels are noisy and this noise can easily corrupt predicted anomalies. We found a significant correlation ($p < 0.01$) between the absolute fAPAR anomalies and the absolute residuals of observed and modeled GPP anomalies at site level, which explained about 13% of the variability (not shown). Inaccurate or insufficiently precise tower coordinates may also lead to the extraction of the wrong fAPAR time series for a tower. Additionally, a mismatch between the satellite pixel and tower footprint can contribute to apparently poor prediction of anomalies, for example if crop fields are harvested that are present in a satellite pixel used for a forest site. We used 2 km fAPAR data from SeaWiFS, while flux towers have a footprint with a length of several ten (short vegetation) to several hundred (forests) meters. The tower footprint may not be representative of the larger SeaWiFS pixel, and errors will result if the mean fAPAR of the satellite pixel is significantly different from that of the tower footprint, especially if this difference is systematically biased across sites. However, the noise of remotely sensed data rapidly diminishes when aggregating to coarser spatial resolution as used for global predictions. Some important questions remain unanswered but need to be kept in mind: (1) How much information is in monthly anomalies of FLUXNET data and what fraction of the variance is actually explainable? (2) To what extent can algorithms like MTE extract the noise in the training data and uncover robust patterns, i.e., are the predicted anomalies more robust than they appear in the cross validation?

[30] The mismatch of MTE predicted and observed anomalies of fluxes are certainly not only caused by uncertainties in the data set. We are also lacking relevant information to predict the anomalies of fluxes accurately. In terms of meteorological variables, we did not use radiation or vapor pressure deficit as explanatory variables (for reasons discussed earlier), and this introduced uncertainties in the prediction of flux anomalies. Moreover, ecosystem responses may lag for some external forcings or respond to a cumulative effect such as a drought that developed over the course of a season [*van der Molen et al.*, 2011] and such effects are not explicitly encoded in the used explanatory variables. Other factors such as management activities (e.g., crop rotations, irrigation, fertilization) and disturbances have also not been considered which likely explains some of the mismatch regarding anomalies, in particular for crops and managed forests. Moreover, site-specific peculiarities such as root groundwater access in dry environments can clearly not be accounted for.

[31] We show that setting up the cross validation in a way where only parts of the time series for each tower site (cross-validation experiment 2, see section 2.5) are predicted for sites yields overly optimistic and misleading results (compare Figures 1 and 2). Cross-validation experiment 2 reveals MEf = 0.79 for among-site variability of NEE as compared to 0.32 for cross-validation experiment 1, and MEf values for among-site variability between 0.93 and 0.96 for the other fluxes in comparison to 0.64–0.86 in cross-validation experiment 2. Cross-validation setups similar to cross-validation experiment 2 are not appropriate for upscaling exercises where the aim is to extrapolate to new locations.

### 3.2. Mean Annual Fluxes

[32] We estimate the global GPP as 119 ± 6 Pg C $yr^{-1}$ for the period 1982–2008, which is consistent with the estimate given in the IPCC AR4 [*Denman et al.*, 2007] of 120 Pg C $yr^{-1}$ and a recent multimodel analysis based on FLUXNET data of 123 ± 8 Pg C $yr^{-1}$ [*Beer et al.*, 2010], where our estimate was one of five included. Our global TER estimate is 96 ± 6 Pg C $yr^{-1}$. To our knowledge, this is the first time that global TER has been quantified independently. Our TER estimate differs from the likely range of

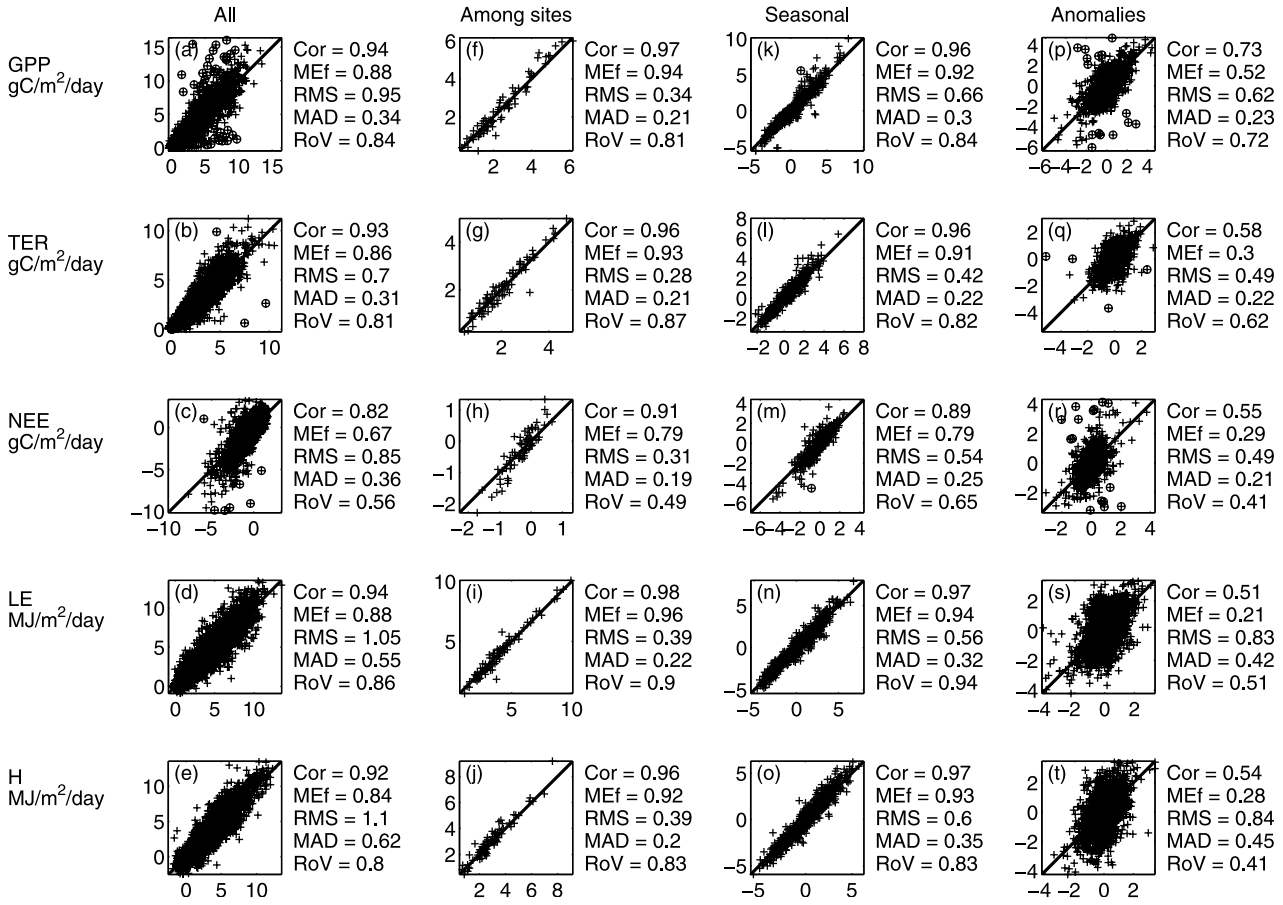


**Figure 2.** MTE predicted (*y* axis) versus FLUXNET observed (*y* axis) GPP, TER, NEE, LE, and H fluxes with performance measures for cross-validation experiment 2 (see section 2.5) for (a–e) all data points, (f–j) among-site variability, (k–o) seasonal variability, and (p–t) anomalies. Outliers are labeled with a circle and were not considered in the calculation of performance measures.

~100–110 Pg C $yr^{-1}$ that is inferred from the residual of the carbon balance equation using equation (3) and literature based estimates of the other remaining component fluxes (Table 2):

$$TER = GPP - NBP - F - LUC - CH - DC - VOC \quad (3)$$

(see Table 2 for definition of terms).

[33] If we assume the values in Table 2 to be correct, then our global TER estimate derived from upscaling FLUXNET data seems to be lower by ~5–10%. It is worth noting here that the global TER estimate based on the flux partitioning according to *Lasslop et al.* [2010] yields only a slightly larger global value of 98 ± 7 Pg C $yr^{-1}$. Our apparent underestimation of TER at the global scale likely originates from a biased sampling of ecosystems, most of which are not in equilibrium with respect to carbon, particularly forests which store large amounts of carbon and undergo natural and human disturbances. Moreover, a small but systematic bias in an eddy covariance derived flux of 8 g C $m^{-2}$ $yr^{-1}$ propagates to 1 Pg C $yr^{-1}$ at the global scale, which illustrates the accuracy requirements of FLUXNET data for estimating global annual means.

[34] Estimated global NEE based on the difference of TER and GPP is −24 Pg C $yr^{-1}$. This estimate carries the

**Table 2.** Synthesis of Global Carbon Balance Component Fluxes and Inferred Flux of Mean Annual Global Terrestrial Ecosystem Respiration

| Carbon Balance Component Flux | Values (Pg C $yr^{-1}$) | Method | Reference |
|---|---|---|---|
| Gross Primary Production (GPP) | 123 ± 8 | Data-oriented models using FLUXNET | *Beer et al.* [2010] |
| Net Biome Production (NBP) | 2.6 ± 1 | Atmospheric inversions | *Denman et al.* [2007] |
| Fire emissions (F) | 1.7–2.5 | Diagnostic and process models | *Thonicke et al.* [2010] |
| Land use change emissions (LUC) | 1.5 | Inventories | *Houghton* [2008] |
| Crop Harvest (CH) | 6–9 | Process model | *Bondeau et al.* [2007] |
| Dissolved organic and inorganic carbon (DC) | 2.9 | Inventories | *Tranvik et al.* [2009] |
| Volatile organic compounds (VOC) | 1.2 | Empirical model | *Guenther et al.* [1995] |
| Terrestrial ecosystem respiration (TER) | ~100–110 | residual | |

**Table 3.** Global Mean Annual Carbon and Energy Fluxes of the Vegetated Land Surface ($127.9 \times 10^6$ km$^2$)[a]

| Carbon Fluxes | Mean (g C m$^{-2}$ yr$^{-1}$) | Total (Pg C yr$^{-1}$) |
|---|---|---|
| Gross primary production (GPP) | 933 ± 46 | 119.4 ± 5.9 |
| Terrestrial ecosystem respiration (TER) | 753 ± 47 | 96.4 ± 6.0 |
| Net ecosystem exchange (NEE) | −133 ± 37 | −17.1 ± 4.7 |
| **Energy Fluxes** | **Mean (MJ m$^{-2}$ yr$^{-1}$)** | **Total (ZJ)** |
| Latent heat (LE) | 1239 ± 54 | 158 ± 7 |
| Sensible heat (H) | 1280 ± 117 | 164 ± 15 |

[a]Uncertainty estimates refer to one standard deviation and are derived from the spread of individual model trees.

likely bias included in our estimated global TER such that the NEE estimate is also likely too low (too negative) by 5–10 Pg C yr$^{-1}$. A second approach of direct upscaling of NEE using MTE yields −17 ± 5 Pg C yr$^{-1}$. Using a third approach based on the flux estimates in Table 2 and equation (4), we infer a global NEP of 15–21 Pg C yr$^{-1}$. Although the independently derived NEP estimate and the upscaling derived NEP estimate appear to be generally consistent, MTE does not yet yield reliable spatially explicit estimates of mean NEP (see section 3.1) because several relevant predictors are lacking, e.g., soil and site history related variables.

$$\mathrm{NEP} = \mathrm{NBP} + \mathrm{F} + \mathrm{LUC} + \mathrm{CH} + \mathrm{DC} + \mathrm{VOC} \quad (4)$$

See Table 2 for definition of terms.

[35] Our estimated mean latent heat flux of $158 \pm 7 \times 10^{18}$ J yr$^{-1}$, equivalent to 39 ± 2 W m$^{-2}$, and to a water flux of $65 \pm 3 \times 10^3$ km$^3$ yr$^{-1}$ agrees with independent global estimates: $66 \times 10^3$ km$^3$ yr$^{-1}$ [*Oki and Kanae*, 2006]; 38.5 W m$^{-2}$ [*Trenberth et al.*, 2009]; 58–85 $\times 10^3$ km$^3$ yr$^{-1}$ [*Dirmeyer et al.*, 2006]; 37–59 W m$^{-2}$ [*Jiménez et al.*, 2011]. The global sensible heat flux of $164 \pm 15 \times 10^{18}$ J yr$^{-1}$ (41 ± 4 W m$^{-2}$) is larger than the value reported by *Trenberth et al.* [2009] (27 W m$^{-2}$) but in the range of various state of the art estimates of the global mean sensible heat flux of 18 to 57 W m$^{-2}$ [*Jiménez et al.*, 2011]. Global mean annual values of estimated biosphere-atmosphere fluxes are summarized in Table 3.

### 3.3. Spatial Distribution of Mean Annual Biosphere-Atmosphere Fluxes

[36] The global spatial distribution of mean annual GPP, TER, and LE are similar with largest fluxes occurring in the equatorial tropics followed by monsoonal subtropical regions (e.g., south and east Asia), and humid temperate regions in eastern North America, and western and central Europe (Figure 3). Small GPP, TER, and LE fluxes occur in cold and dry environments. The similarity of spatial GPP, TER, and LE patterns results from their intimate coupling: GPP provides substrate for respiration and is thus the first order factor controlling TER which has been shown in various studies [e.g., *Lasslop et al.*, 2010], GPP and LE are closely linked since a certain amount of water needs to be transpired to fix a certain amount of carbon during photosynthesis (water use efficiency), and because evaporation of intercepted rain depends on LAI as does GPP.

[37] The global spatial distribution of H shows the largest values in subtropical dry regions where available energy is preferentially partitioned to H rather than LE. We infer that the median evaporative fraction, here defined as LE/(LE+H), is 0.47 and varies spatially from 0.01 in very dry areas to 0.78 in very humid regions (95% range, map not shown).

[38] A quantitative comparison of the upscaled mean annual LE against catchment water balances, and land surface model simulations shows strong consistency ($R^2$ of 0.92 for catchment water balances and 0.91 for ensemble of land surface models [*Jung et al.*, 2010]). A detailed multimodel comparison of global H and LE flux estimates including those presented here is available from *Jiménez et al.* [2011].

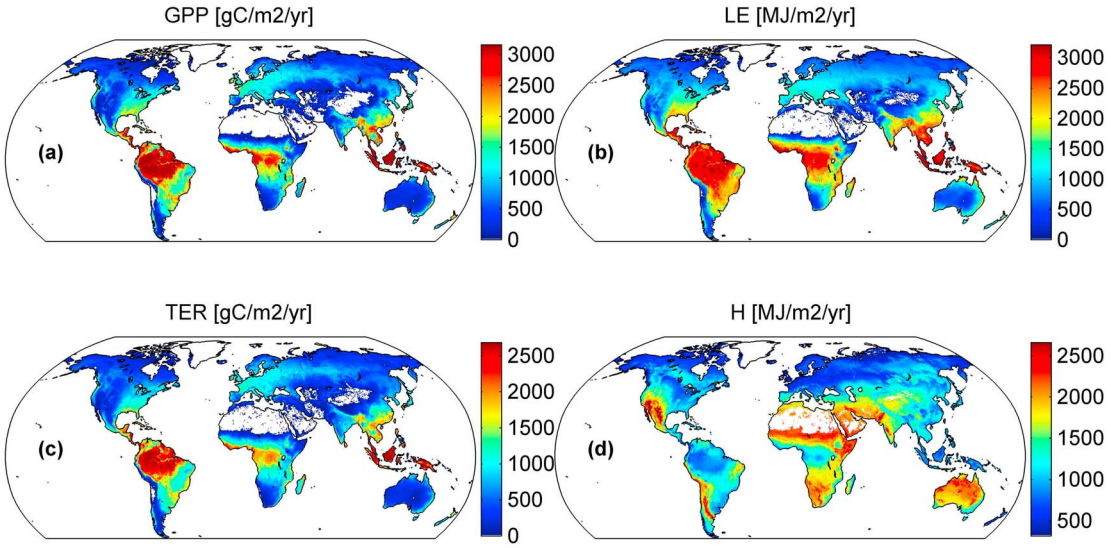


**Figure 3.** Mean annual (1982–2008) (a) GPP, (b) LE, (c) TER, and (d) H derived from global empirical upscaling of FLUXNET data.

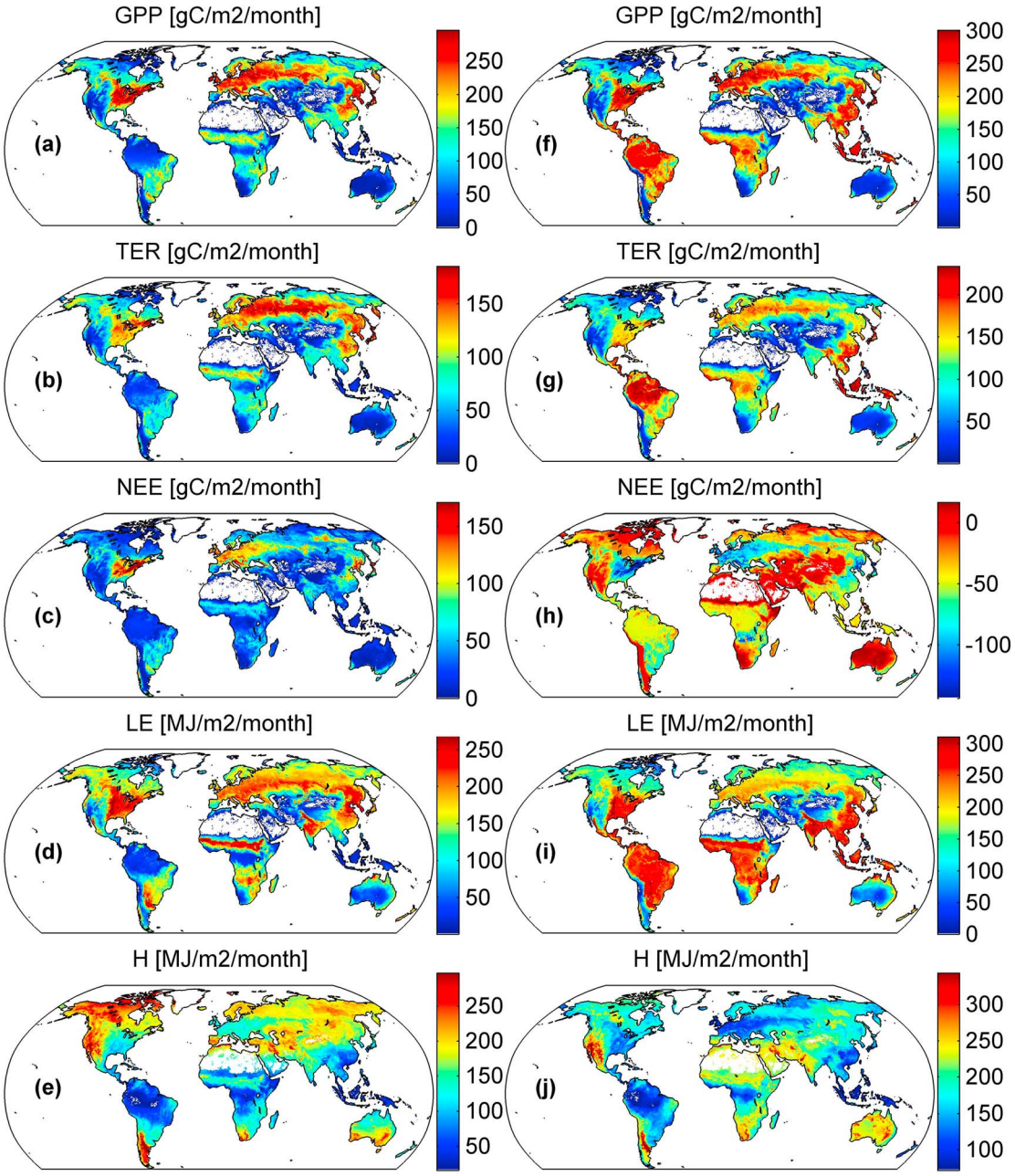


**Figure 4.** Amplitude of the mean seasonal cycle of (a–e) GPP, TER, NEE, LE, and H and (f–j) maximum monthly flux of the mean seasonal cycle calculated for the period 1982–2008. In the case of NEE (Figure 4h), the minimum flux, i.e., largest uptake by land, is plotted.

### 3.4. Patterns of Seasonal Variation of Carbon and Energy Fluxes

[39] *Huston and Wolverton* [2009] suggested that mean and maximum net primary productivity (NPP) of temperate ecosystems is at least as large as in the tropics. Furthermore, temperate rain forest regions (e.g., Pacific Northwest America) have biomass and NPP values similar to that of tropical rain forests [*Hudiburg et al.*, 2009]. For GPP, we find that some temperate regions in eastern North America and Eurasia indeed exhibit a similarly high or even larger maximum GPP during northern hemisphere summer months (June, July) compared to rates in the tropics (Figure 4f). Approximately the same regions also show the largest amplitude of the GPP mean seasonal cycle (Figure 4a). In contrast to the seasonal northern hemisphere GPP maxima, the mean maximum TER is largest in the South American and East Asian tropics with substantially smaller maximum TER in temperate regions, but also in tropical Africa (Figure 4g). The largest amplitudes of the TER mean seasonal cycle is in northern Eurasia, where also the amplitude of the GPP mean seasonal cycle is large resulting in a smaller amplitude of the NEE seasonal cycle compared to Europe

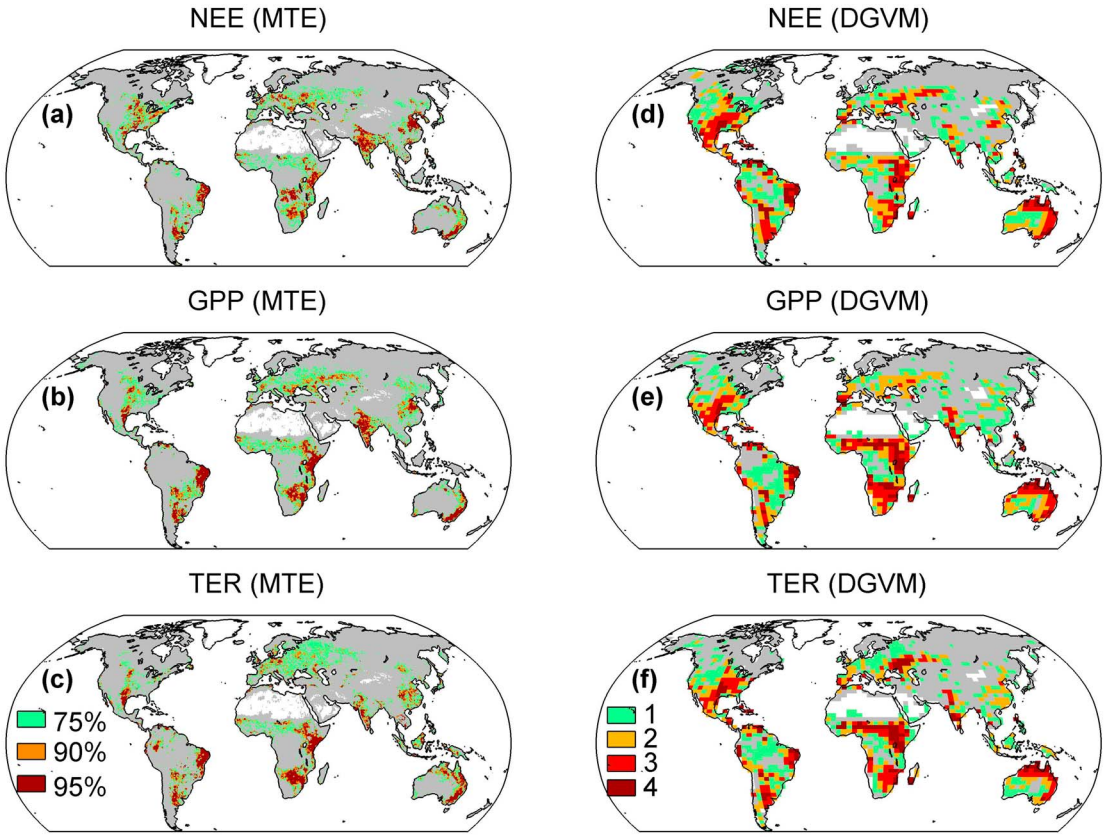


**Figure 5.** Hot spot regions of interannual variability of NEE, GPP, and TER based on (a–c) upscaling and (d–f) DGVMs. Figures 5a–5c show regions where the standard deviation of annual sums exceeds the 75th, 90th, and 95th percentiles; Figures 5d–5f show maps with the number of models where the standard deviation exceed the 75th percentile.

(Figures 4a, 4b, and 4c). We find the mean minimum NEE of the year (i.e., largest uptake) is in eastern North America and Western Europe primarily during the early growing season (May–July) and these regions also show the largest amplitude of the NEE mean seasonal cycle (Figures 4c and 4h).

[40] Our analysis shows the largest amplitude of the mean seasonal cycle of LE for eastern North America, the savannas of northern Africa, and South Asia (e.g., central India) (Figure 4d). Some of the regions with the largest amplitude of the annual LE cycle also correspond to the largest monthly LE fluxes of the year, i.e., in the savannas of northern Africa, parts of South Asia and North America (Figure 4i). Thus, maximum LE fluxes within the year of some warm environments that have a pronounced rainy season seem to exceed the maximum LE flux in the year of the humid tropics, possibly because high maximum surface conductance during the wet season, e.g., C4 grass vegetation.

### 3.5. Hot Spots of Interannual Variability of Carbon Fluxes

[41] Where are the global hot spot regions of interannual variability of carbon fluxes? We calculated the standard deviation of annual carbon flux sums for each pixel to measure the interannual variability and mapped regions where the standard deviation exceeds the 75th, 90th, and 95th percentile of the global distribution of standard deviations, which we refer to as hot spot regions (Figures 5a–5c). We find hot spots of NEE interannual variability in eastern and southern South America, eastern and southern Africa, Southeast Asia (e.g., India, eastern China), southeastern Australia, central and eastern North America and in Europe (Figure 5a). Many regions with large interannual variability are not well covered by FLUXNET sites and our cross-validation results indicated substantial uncertainty of predicted monthly NEE anomalies (see section 3.1). For this reason, we corroborate our findings with results from four dynamical global vegetation models (DGVMs) for the same time period (1982–2008) used by *Le Quéré et al.* [2009]: LPJ [*Sitch et al.*, 2003], Triffid [*Cox*, 2001], SDGVM [*Woodward et al.*, 1995], and HyLand [*Levy et al.*, 2004].

[42] The four DGVMs were forced with the same meteorological data. At each pixel, we counted how many of the models indicate a hot spot region of interannual variability, defined by exceeding the 75th percentile of the global, model specific distribution of standard deviations. The global spatial pattern of hot spot regions of interannual variability of NEE derived from the upscaling is largely consistent with the pattern predicted by the ensemble of four DGVMs (Figure 5d). Some discrepancies between the upscaled product and DGVMs are expected to arise from different meteorological forcing data, and because DGVMs simulate LAI while remotely sensed fAPAR is used in the

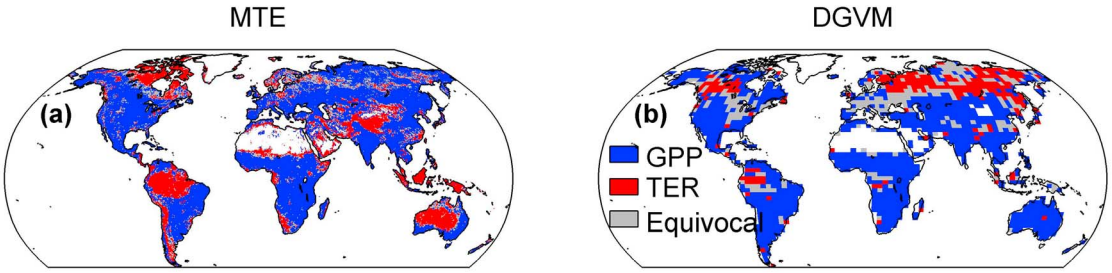


**Figure 6.** Maps showing where GPP or TER interannual variability is more strongly related to NEE interannual variability based on (a) upscaling and (b) DGVMs. For the DGVMs the majority estimate of the four models is plotted where "equivocal" refers to situations where no majority exists.

upscaling. Both the MTE and DGVM runs discussed here essentially reflect variability due to climate but were not designed to capture variability due to land use change. Therefore, the interannual variability may be underestimated by MTE and DGVMs in regions with extensive land use change but the overall spatial pattern of hot spots is likely not affected by this.

[43] The global pattern of NEE interannual variability shares several features with climate anomalies associated with El Nino–Southern Oscillation, which has been shown to correlate with interannual variations of global land carbon uptake estimated by atmospheric inversions [*Gurney et al.*, 2008]. For example, interannual variability tends to be large in regions known to experience climate anomalies during at least some ENSO events [e.g., *Williams and Hanan*, 2011], such as northern and eastern Australia, southern Africa and equatorial East Africa, southeastern South America, and eastern North America. The spatial patterns of GPP and TER interannual variability are roughly consistent with the global pattern of NEE interannual variability, which is also simulated in the four DGVMs (Figure 5). Nevertheless the absolute magnitude of the interannual variability is considerably lower in the MTE compared to the DGVMs (not shown). Combined with the cross-validation results, this indicates that the current MTE version may underestimate the interannual variability.

[44] Is the interannual variability of NEE predominantly related to GPP or TER variations? We calculated the variances of annual sums of GPP and TER for each pixel to determine if interannual variability of NEE is more dominated by interannual variability of GPP or TER. We mapped GPP as dominant control if the variance of annual GPP is 20% larger than the variance of annual TER (and accordingly for TER). For the majority of the land surface, we find that the interannual variability of NEE is dominated by interannual variations of GPP (Figure 6a), which is consistent with some regional to continental studies for Europe [*Ciais et al.*, 2005; *Luyssaert et al.*, 2007; *Vetter et al.*, 2008], and Africa [*Weber et al.*, 2009]. Global simulations by DGVMs also suggest that GPP variability drives NEE variability in most regions of the world (Figure 6b). DGVM simulations and our upscaling product are consistent in that GPP drives NEE interannual variations in the identified hot spot regions of interannual variability. We find that TER appears to drive NEE interannual variations in the South American and East Asian tropics, which is to some extent also suggested by the DGVMs. Here, the interannual variability of TER is larger than the interannual variability of GPP, probably because photosynthesis is not strongly limited by climatic conditions.

[45] A major discrepancy between our upscaled product and DGVM simulations regarding the dominant process controlling interannual variations of NEE is apparent in large parts of the boreal zone that experienced the strongest warming over the last decades, DGVMs indicate respiration as the dominant process. In these regions, the DGVM simulations depend critically on the parameterization of the temperature sensitivity of respiration [*Jones et al.*, 2003]. Recent results suggest that this temperature sensitivity could be overestimated in the models [*Frank et al.*, 2010; *Mahecha et al.*, 2010]. In contrast to the DGVMs, MTE suggests TER as dominant component of NEE interannual

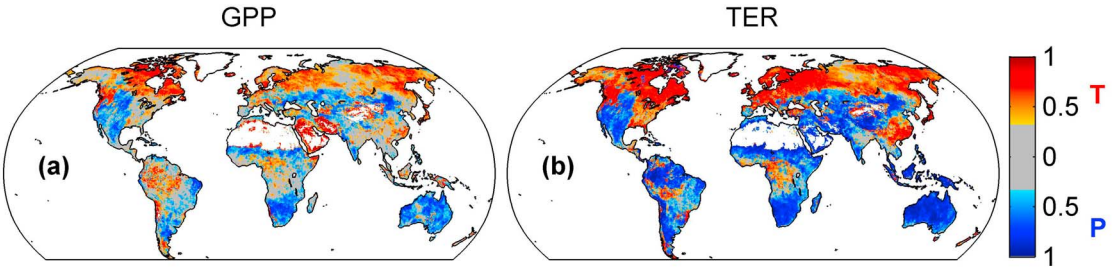


**Figure 7.** (a) Maximum value composite map of Pearson's correlation coefficients between annual GPP and temperature (red scale) and precipitation (blue scale) and (b) for TER accordingly. Gray areas indicate nonsignificant correlations ($p > 0.1$).

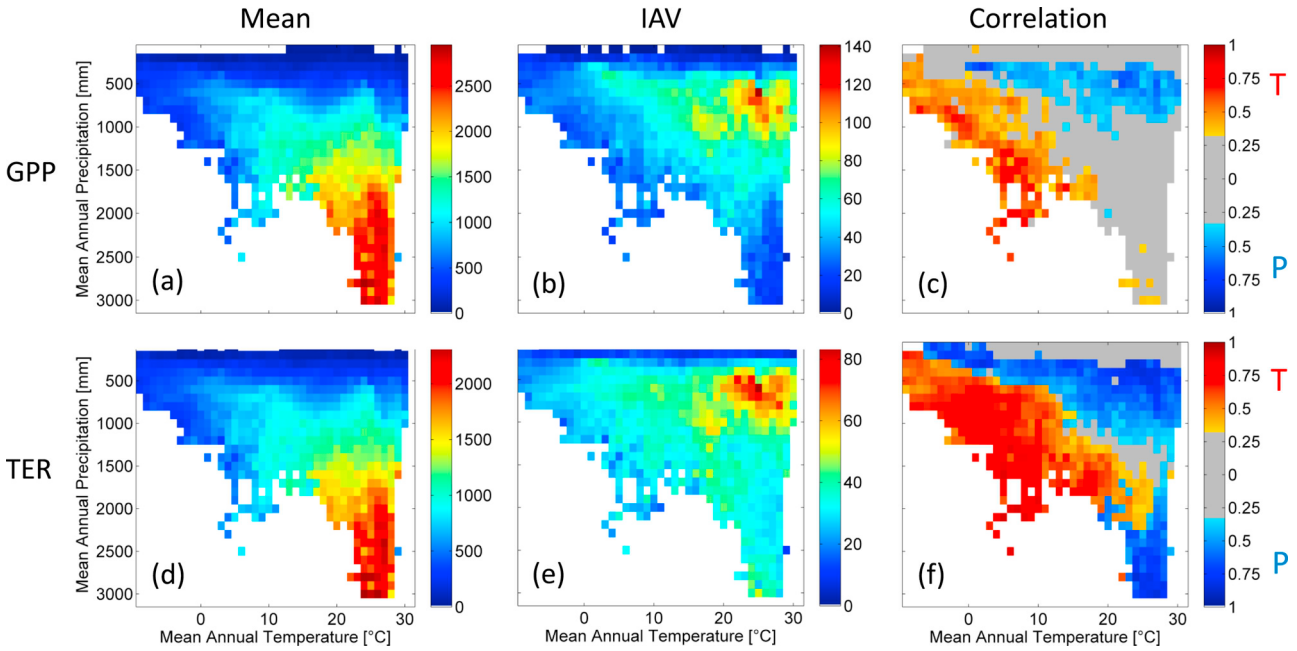


**Figure 8.** (a) Mean annual GPP, (b) interannual variability of GPP, and (c) majority maximum interannual correlation with temperature (red scale) and precipitation (blue scale; see Figure 7) in climate space. (d–f) Same as Figure 8a except for TER.

variability in some very dry regions (e.g., Australia) and the arctic region of North America. Given that uncertainties of the interannual variability of fluxes are substantial in both approaches, it remains an open question whether MTE or DGVMs deliver the correct pattern.

[46] Where do temperature or precipitation variations explain the interannual variations of GPP and TER? Interannual variations of GPP and TER are more strongly correlated with interannual variations in precipitation in subtropical regions (Figure 7). The interannual variability of GPP and TER in cold, cool, and humid regions is overall more strongly correlated with temperature. In some tropical regions where TER interannual variations seem to dominate NEE interannual variability, TER interannual variability is more strongly correlated with precipitation than with temperature, while GPP is more strongly correlated with temperature (likely because these forests are radiation limited). It is possible that soil respiration in tropical domains is much more limited by the moisture content of the litter than by temperature. By analyzing the interannual variability of GPP and TER and their predominant correlation with temperature or precipitation in climate space, we can see clearly that the hot spot regions of interannual variability of land atmosphere fluxes falls in the climatic domain where moisture supply seems to be the primary driver of the variability (Figure 8). Within the range of ~20–30°C and ~500–1000 mm where GPP and TER interannual variability are largest, both GPP and TER are more strongly positively correlated with precipitation than with temperature. Thus, the interannual variability of biosphere-atmosphere fluxes peaks in semiarid to semihumid regions where mean rainfall allows sustaining sufficient biological activity, which, however, remains very sensitive to rainfall variations [e.g., *Knapp and Smith*, 2001]. Such transitional zones appear to be key players of atmosphere-biosphere interactions as was previously illustrated by *Koster et al.* [2004] showing the impact of soil moisture anomalies in such regions on regional precipitation patterns.

## 4. Summary and Conclusions

[47] We developed a method for upscaling observations of biosphere-atmosphere fluxes of carbon and energy from eddy covariance flux tower sites (FLUXNET) to the global scale and presented an initial exploratory analysis of the resulting global patterns of biosphere-atmosphere fluxes. Globally integrated values of GPP, LE and H, derived from upscaling FLUXNET data, were broadly consistent with independent estimates, though we inferred a possible 5–10% underestimation of our global TER estimates with consequent effects on our calculation of global NEE. The global spatial distributions of GPP, TER, and LE showed similar patterns due to their close mechanistic connections, with the largest fluxes occurring in the humid tropics and the smallest fluxes in cold and dry environments. Global patterns of maximum monthly GPP indicated that some temperate regions have a similar or higher seasonal peak productivity than the inner tropics. We also observed the largest annual LE fluxes in some rainy season-dominated ecosystems, even exceeding that in the humid tropics. We identified semiarid to subhumid regions as global hot spots of interannual variability in carbon fluxes, with a global spatial pattern that is consistent with simulations of four DGVMs. In these regions, the interannual variability of carbon fluxes appeared to be dominated by interannual rainfall variations, emphasizing the importance of the water cycle in driving global biogeochemical cycles. We inferred that the interannnual

variability of GPP dominates the interannual variability of NEE in most regions of the world with notable exceptions in some tropical areas where TER seems to drive NEE interannual variations. DGVMs suggested that a larger fraction of interannual variability in NEE is driven by respiration across large parts of the boreal zone as compared to our data-driven analysis.

[48] Our upscaling approach integrated a large body of in situ measurements, remote sensing and meteorological observations using a machine learning technique. This approach is independent from and complementary to process-oriented modeling. The data sets provided by this analysis can be used for exploratory analysis and generation of hypotheses, diagnostic assessments, and corroboration against process model simulations. Clearly, the comparison of process model simulations with diagnostic patterns can provide valuable insights for advancing and improving both approaches. Upscaling is still hampered by a variety of challenges such as limited ability to account for effects of disturbance and/or site history, and lagged environmental effects. The field of global upscaling of biosphere-atmosphere fluxes is fairly new, and future improvements—in terms of statistical approaches, predictor data, and global coverage distribution of FLUXNET tower sites—are expected to offer valuable advances in our ability to diagnose the state of the biosphere from observational data streams.

[49] **Acknowledgments.** This work used eddy covariance data acquired by the FLUXNET community and in particular by the following networks: AmeriFlux (U.S. Department of Energy, Biological and Environmental Research, Terrestrial Carbon Program (DE-FG02-04ER63917 and DE-FG02-04ER63911)), AfriFlux, AsiaFlux, CarboAfrica, CarboEuropeIP, CarboItaly, CarboMont, ChinaFlux, FLUXNET Canada (supported by CFCAS, NSERC, BIOCAP, Environment Canada, and NRCan), GreenGrass, KoFlux, LBA, NECC, OzFlux, TCOS-Siberia, USCCC. We acknowledge the financial support to the eddy covariance data harmonization provided by CarboEuropeIP, FAO-GTOS-TCO, iLEAPS, Max Planck Institute for Biogeochemistry, National Science Foundation, University of Tuscia, Université Laval, Environment Canada and U.S. Department of Energy and the database development and technical support from Berkeley Water Center, Lawrence Berkeley National Laboratory, Microsoft Research eScience, Oak Ridge National Laboratory, University of California Berkeley, University of Virginia. M.J. and M.R. were supported by the European Union (FP7) Integrated projects COMBINE (226520), CIRCE (036961) and a grant from the Max-Planck Society to the MPRG Biogeochemical Model-Data Integration. C.A.W. was supported by the U.S. National Science Foundation under grant ATM-0910766. D.P. thanks the support of CMCC.

## References

Amiro, B. D., et al. (2010), Ecosystem carbon dioxide fluxes after disturbance in forests of North America, *J. Geophys. Res.*, *115*, G00K02, doi:10.1029/2010JG001390.

Aubinet, M. (2008), Eddy covariance $CO_2$ flux measurements in nocturnal conditions: An analysis of the problem, *Ecol. Appl.*, *18*, 1368–1378, doi:10.1890/06-1336.1.

Baldocchi, D. (2008), 'Breathing' of the terrestrial biosphere: Lessons learned from a global network of carbon dioxide flux measurement systems, *Aust. J. Bot.*, *56*, 1–26, doi:10.1071/BT07151.

Baldocchi, D., et al. (2001), FLUXNET: A new tool to study the temporal and spatial variability of ecosystem-scale carbon dioxide, water vapor, and energy flux densities, *Bull. Am. Meteorol. Soc.*, *82*, 2415–2434, doi:10.1175/1520-0477(2001)082<2415:FANTTS>2.3.CO;2.

Barr, A. G., K. Morgenstern, T. A. Black, J. H. McCaughey, and Z. Nesic (2006), Surface energy balance closure by the eddy-covariance method above three boreal forest stands and implications for the measurement of the $CO_2$ flux, *Agric. For. Meteorol.*, *140*, 322–337, doi:10.1016/j.agrformet.2006.08.007.

Beer, C., et al. (2010), Terrestrial gross carbon dioxide uptake: Global distribution and covariation with climate, *Science*, *329*, 834–838, doi:10.1126/science.1184984.

Bondeau, A., et al. (2007), Modelling the role of agriculture for the 20th century global terrestrial carbon balance, *Global Change Biol.*, *13*, 679–706, doi:10.1111/j.1365-2486.2006.01305.x.

Braswell, B. H., W. J. Sacks, E. Linder, and D. Schimel (2005), Estimating diurnal to annual ecosystem parameters by synthesis of a carbon flux model with eddy covariance net ecosystem exchange observations, *Global Change Biol.*, *11*, 335–355, doi:10.1111/j.1365-2486.2005.00897.x.

Carvalhais, N., et al. (2008), Implications of the carbon cycle steady state assumption for biogeochemical modeling performance and inverse parameter retrieval, *Global Biogeochem. Cycles*, *22*, GB2007, doi:10.1029/2007GB003033.

Ciais, P., et al. (2005), Europe-wide reduction in primary productivity caused by the heat and drought in 2003, *Nature*, *437*, 529–533, doi:10.1038/nature03972.

Cox, P. (2001), Description of the 'TRIFFID' dynamic global vegetation model, *Tech. Note 24*, Hadley Cent., Exeter, U. K.

Denman, K. L., et al. (2007), Couplings between changes in the climate system and biogeochemistry, in *Climate Change 2007: The Physical Science Basis. Contribution of Working Group I to the Fourth Assessment Report of the Intergovernmental Panel on Climate Change*, edited by S. Solomon et al., pp. 499–587, Cambridge Univ. Press, Cambridge, U. K.

Dirmeyer, P. A., et al. (2006), The Second Global Soil Wetness Project (GSWP-2), Multi-model analysis and implications for our perception of the land surface, *Bull. Am. Meteorol. Soc.*, *87*, 1381–1397, doi:10.1175/BAMS-87-10-1381.

Foken, T. (2008), The energy balance closure problem: An overview, *Ecol. Appl.*, *18*, 1351–1367, doi:10.1890/06-0922.1.

Frank, D. C., J. Esper, C. C. Raible, U. Buntgen, V. Trouet, B. Stocker, and F. Joos (2010), Ensemble reconstruction constraints on the global carbon cycle sensitivity to climate, *Nature*, *463*, 527–530, doi:10.1038/nature08769.

Friedlingstein, P., et al. (2006), Climate-carbon cycle feedback analysis: Results from the $C^4MIP$ model intercomparison, *J. Clim.*, *19*, 3337–3353, doi:10.1175/JCLI3800.1.

Gobron, N., et al. (2006), Evaluation of fraction of absorbed photosynthetically active radiation products for different canopy radiation transfer regimes: Methodology and results using Joint Research Center products derived from SeaWiFS against ground-based estimations, *J. Geophys. Res.*, *111*, D13110, doi:10.1029/2005JD006511.

Gobron, N., et al. (2008), Uncertainty estimates for the FAPAR operational products derived from MERIS: Impact of top-of-atmosphere radiance uncertainties and validation with field data, *Remote Sens. Environ.*, *112*, 1871–1883 doi:10.1016/j.rse.2007.09.011.

Guenther, A., et al. (1995), A global model of natural volatile organic compound emissions, *J. Geophys. Res.*, *100*, 8873–8892, doi:10.1029/94JD02950.

Gurney, K. R., et al. (2008), Interannual variations in continental-scale net carbon exchange and sensitivity to observing networks estimated from atmospheric $CO_2$ inversions for the period 1980 to 2005, *Global Biogeochem. Cycles*, *22*, GB3025, doi:10.1029/2007GB003082.

Hendricks Franssen, H. J., et al. (2010), Energy balance closure of eddy-covariance data: A multisite analysis for European FLUXNET stations, *Agric. For. Meteorol.*, *150*, 1553–1567, doi:10.1016/j.agrformet.2010.08.005.

Hicke, J. A. (2005), NCEP and GISS solar radiation data sets available for ecosystem modeling: Description, differences, and impacts on net primary production, *Global Biogeochem. Cycles*, *19*, GB2006, doi:10.1029/2004GB002391.

Houghton, R. A. (2008), Carbon flux to the atmosphere from land-use changes: 1850–2005, report, Carbon Dioxide Inf. Anal. Cent., Oak Ridge Natl. Lab., U.S. Dep. of Energy, Oak Ridge, Tenn.

Hudiburg, T., B. Law, D. P. Turner, J. Campbell, D. Donato, and M. Duane (2009), Carbon dynamics of Oregon and northern California forests and potential land-based carbon storage, *Ecol. Appl.*, *19*, 163–180, doi:10.1890/07-2006.1.

Huston, M. A., and S. Wolverton (2009), The global distribution of net primary production: Resolving the paradox, *Ecol. Monogr.*, *79*, 343–377, doi:10.1890/08-0588.1.

Jiménez, C., et al. (2011), Global intercomparison of 12 land surface heat flux estimates, *J. Geophys. Res.*, *116*, D02102, doi:10.1029/2010JD014545.

Jones, C. D., et al. (2003), Uncertainty in climate–carbon-cycle projections associated with the sensitivity of soil respiration to temperature, *Tellus, Ser. B*, *55*, 642–648, doi:10.1034/j.1600-0889.2003.01440.x.

Jung, M., et al. (2006), Exploiting synergies of global land cover products for carbon cycle modeling, *Remote Sens. Environ.*, *101*, 534–553, doi:10.1016/j.rse.2006.01.020.

Jung, M., et al. (2007a), Assessing the ability of three land ecosystem models to simulate gross carbon uptake of forests from boreal to Mediterranean climate in Europe, *Biogeosciences*, *4*, 647–656, doi:10.5194/bg-4-647-2007.

Jung, M., et al. (2007b), Uncertainties of modeling gross primary productivity over Europe: A systematic study on the effects of using different drivers and terrestrial biosphere models, *Global Biogeochem. Cycles*, *21*, GB4021, doi:10.1029/2006GB002915.

Jung, M., et al. (2009), Towards global empirical upscaling of FLUXNET eddy covariance observations: Validation of a model tree ensemble approach using a biosphere model, *Biogeosciences*, *6*, 2001–2013, doi:10.5194/bg-6-2001-2009.

Jung, M., et al. (2010), Recent decline in the global land evapotranspiration trend due to limited moisture supply, *Nature*, *467*, 951–954, doi:10.1038/nature09396.

Knapp, A. K., and M. D. Smith (2001), Variation among biomes in temporal dynamics of aboveground primary production, *Science*, *291*, 481–484, doi:10.1126/science.291.5503.481.

Koster, R. D., et al. (2004), Regions of strong coupling between soil moisture and precipitation, *Science*, *305*, 1138–1140, doi:10.1126/science.1100217.

Krinner, G., et al. (2005), A dynamic global vegetation model for studies of the coupled atmosphere-biosphere system, *Global Biogeochem. Cycles*, *19*, GB1015, doi:10.1029/2003GB002199.

Lasslop, G., et al. (2008), Influence of observation errors in eddy flux data on inverse model parameter estimation, *Biogeosciences*, *5*, 1311–1324, doi:10.5194/bg-5-1311-2008.

Lasslop, G., et al. (2010), Separation of net ecosystem exchange into assimilation and respiration using a light response curve approach: Critical issues and global evaluation, *Global Change Biol.*, *16*, 187–208, doi:10.1111/j.1365-2486.2009.02041.x.

Law, B. E., and R. H. Waring (1994), Combining remote sensing and climatic data to estimate net primary production across Oregon, *Ecol. Appl.*, *4*, 717–728, doi:10.2307/1942002.

Le Quéré, C., et al. (2009), Trends in the sources and sinks of carbon dioxide, *Nat. Geosci.*, *2*, 831–836, doi:10.1038/ngeo689.

Levy, P. E., et al. (2004), Modelling the impact of future changes in climate, $CO_2$ concentration and land use on natural ecosystems and the terrestrial carbon sink, *Glob. Environ. Change*, *14*, 21–30, doi:10.1016/j.gloenvcha.2003.10.005.

Luyssaert, S., et al. (2007), Photosynthesis drives anomalies in net carbon-exchange of pine forests at different latitudes, *Global Change Biol.*, *13*, 2110–2127, doi:10.1111/j.1365-2486.2007.01432.x.

Mahecha, M. D., et al. (2010), Global convergence in the temperature sensitivity of respiration at ecosystem level, *Science*, *329*, 838–840, doi:10.1126/science.1189587.

Moffat, A. M., et al. (2007), Comprehensive comparison of gap-filling techniques for eddy covariance net carbon fluxes, *Agric. For. Meteorol.*, *147*, 209–232, doi:10.1016/j.agrformet.2007.08.011.

Moncrieff, J., et al. (1996), The propagation of errors in long-term measurements of land-atmosphere fluxes of carbon and water, *Global Change Biol.*, *2*, 231–240, doi:10.1111/j.1365-2486.1996.tb00075.x.

Monfreda, C., et al. (2008), Farming the planet: 2. Geographic distribution of crop areas, yields, physiological types, and net primary production in the year 2000, *Global Biogeochem. Cycles*, *22*, GB1022, doi:10.1029/2007GB002947.

Nash, J. E., and J. V. Sutcliffe (1970), River flow forecasting through conceptual models part I: A discussion of principles, *J. Hydrol.*, *10*, 282–290, doi:10.1016/0022-1694(70)90255-6.

New, M., et al. (2002), A high-resolution data set of surface climate over global land areas, *Clim. Res.*, *21*, 1–25, doi:10.3354/cr021001.

Oki, T., and S. Kanae (2006), Global hydrological cycles and world water resources, *Science*, *313*, 1068–1072, doi:10.1126/science.1128845.

Österle, H., et al. (2003), Homogenisierung und Aktualisierung des Klimadatensdatzes der Climate Research Unit of East Anglia, Norwich, *Terra Nostra*, *6*, 326–329.

Papale, D., and A. Valentini (2003), A new assessment of European forests carbon exchanges by eddy fluxes and artificial neural network spatialization, *Global Change Biol.*, *9*, 525–535, doi:10.1046/j.1365-2486.2003.00609.x.

Papale, D., et al. (2006), Towards a standardized processing of Net Ecosystem Exchange measured with eddy covariance technique: Algorithms and uncertainty estimation, *Biogeosciences*, *3*, 571–583, doi:10.5194/bg-3-571-2006.

Piao, S., P. Friedlingstein, P. Ciais, P. Peylin, B. Zhu, and M. Reichstein (2009), Footprint of temperature changes in the temperate and boreal forest carbon balance, *Geophys. Res. Lett.*, *36*, L07404, doi:10.1029/2009GL037381.

Reichstein, M., et al. (2005), On the separation of net ecosystem exchange into assimilation and ecosystem respiration: Review and improved algorithm, *Global Change Biol.*, *11*, 1424–1439, doi:10.1111/j.1365-2486.2005.001002.x.

Richardson, A. D., et al. (2006), A multi-site analysis of random error in tower-based measurements of carbon and energy fluxes, *Agric. For. Meteorol.*, *136*, 1–18, doi:10.1016/j.agrformet.2006.01.007.

Richardson, A. D., et al. (2008), Statistical properties of random $CO_2$ flux measurement uncertainty inferred from model residuals, *Agric. For. Meteorol.*, *148*, 38–50, doi:10.1016/j.agrformet.2007.09.001.

Richardson, A. D., et al. (2010), Estimating parameters of a forest ecosystem C model with measurements of stocks and fluxes as joint constraints, *Oecologia*, *164*, 25–40, doi:10.1007/s00442-010-1628-y.

Running, S. W., and E. R. J. Hunt (1993), Generalization of a forest ecosystem process model for other biomes, BIOME-BGC, and an application for the global scale, in *Scaling Physiological Processes: Leaf to Globe*, edited by J. R. Ehleringer and C. B. Field, pp. 141–158, Academic, San Diego, Calif.

Schneider, U., et al. (2008), Global precipitation analysis products of the GPCC, report, Global Precip. Climatol. Cent., Offenbach, Germany.

Schwarz, G. (1978), Estimating the dimension of a model, *Ann. Stat.*, *6*, 461–464, doi:10.1214/aos/1176344136.

Simmons, A., et al. (2007), ERA-Interim: New ECMWF reanalysis products from 1989 onwards, *ECMWF Newsl.*, *110*, 25–35.

Sitch, S., et al. (2003), Evaluation of ecosystem dynamics, plant geography and terrestrial carbon cycling in the LPJ dynamic global vegetation model, *Global Change Biol.*, *9*, 161–185, doi:10.1046/j.1365-2486.2003.00569.x.

Spadavecchia, L., et al. (2011), Uncertainty in predictions of forest carbon dynamics: Separating driver error from model error, *Ecol. Appl.*, *21*, 1506–1522, doi:10.1890/09-1183.1.

Thonicke, K., et al. (2010), The influence of vegetation, fire spread and fire behaviour on biomass burning and trace gas emissions: Results from a process-based model, *Biogeosciences*, *7*, 1991–2011, doi:10.5194/bg-7-1991-2010.

Tranvik, L. J., et al. (2009), Lakes and reservoirs as regulators of carbon cycling and climate, *Limnol. Oceanogr.*, *54*, 2298–2314, doi:10.4319/lo.2009.54.6_part_2.2298.

Trenberth, K. E., et al. (2009), Earth's global energy budget, *Bull. Am. Meteorol. Soc.*, *90*, 311–323, doi:10.1175/2008BAMS2634.1.

Tucker, C., et al. (2005), An extended AVHRR 8-km NDVI data set compatible with MODIS and SPOT vegetation NDVI data, *Int. J. Remote Sens.*, *26*, 4485–4498, doi:10.1080/01431160500168686.

Twine, T. E., et al. (2000), Correcting eddy-covariance flux underestimates over a grassland, *Agric. For. Meteorol.*, *103*, 279–300, doi:10.1016/S0168-1923(00)00123-4.

van der Molen, M. K., et al. (2011), Drought and ecosystem carbon cycling, *Agric. For. Meteorol.*, doi:10.1016/j.agrformet.2011.01.018.

Vetter, M., et al. (2008), Analyzing the causes and spatial pattern of the European 2003 carbon flux anomaly in Europe using seven models, *Biogeosciences*, *5*, 561–583, doi:10.5194/bg-5-561-2008.

Weber, U., et al. (2009), The inter-annual variability of Africa's ecosystem productivity: A multi-model analysis, *Biogeosciences*, *6*, 285–295, doi:10.5194/bg-6-285-2009.

Williams, C. A., and N. P. Hanan (2011), ENSO and IOD teleconnections for African ecosystems: Evidence of destructive interference between climate oscillations, *Biogeosciences*, *8*, 27–40, doi:10.5194/bg-8-27-2011.

Williams, M., et al. (2009), Improving land surface models with FLUXNET data, *Biogeosciences*, *6*, 1341–1359, doi:10.5194/bg-6-1341-2009.

Wilson, K., et al. (2002), Energy balance closure at FLUXNET sites, *Agric. For. Meteorol.*, *113*, 223–243, doi:10.1016/S0168-1923(02)00109-0.

Winslow, J. C., et al. (2003), The influence of seasonal water availability on global C3 versus C4 grassland biomass and its implications for climate change research, *Ecol. Modell.*, *163*, 153–173, doi:10.1016/S0304-3800(02)00415-5.

Woodward, F. I., et al. (1995), A global land primary productivity and phytogeography model, *Global Biogeochem. Cycles*, *9*, 471–490, doi:10.1029/95GB02432.

Xiao, J. F., et al. (2008), Estimation of net ecosystem carbon exchange for the conterminous United States by combining MODIS and AmeriFlux data, *Agric. For. Meteorol.*, *148*, 1827–1847, doi:10.1016/j.agrformet.2008.06.015.

Yang, L., et al. (2007), Developing a continental-scale measure of gross primary production by combining MODIS and AmeriFlux data through Support Vector Machine Approach, *Remote Sens. Environ.*, *110*, 109–122, doi:10.1016/j.rse.2007.02.016.

Zhao, M., et al. (2006), Sensitivity of moderate resolution imaging spectroradiometer (MODIS) terrestrial primary production to the accuracy of meteorological reanalyses, *J. Geophys. Res.*, *111*, G01002, doi:10.1029/2004JG000004.

M. A. Arain, School of Geography and Earth Sciences, McMaster University, 1280 Main St. W., Hamilton, ON L8S 4K1, Canada.

A. Arneth and A. Lindroth, Division of Physical Geography and Ecosystem Analysis, Department of Earth and Ecosystem Sciences, Lund University, Sölvegatan 12, SE-22362 Lund, Sweden.

C. Bernhofer, Department of Meteorology, Institute of Hydrology and Meteorology, Technische Universität, Pressestelle, D-01062 Dresden, Germany.

D. Bonal, INRA, UMR INRA-UHP 1137 Ecologie et Ecophysiologie Forestière, F-54280 Champenoux, France.

A. Cescatti, Climate Change and Air Quality Unit, Institute for Environment and Sustainability, Joint Research Centre, European Commission, Via E. Fermi 2749, I-21027 Ispra (VA), Italy.

J. Chen, Department of Environmental Sciences, University of Toledo, Mail Stop 604, Toledo, OH 43606, USA.

D. Gianelle and M. Sottocornola, Environment and Natural Resources Area, Research and Innovation Centre, IASMA, Fondazione Edmund Mach, Viote del Bondone, Trento, I-38100 Trento, Italy.

N. Gobron, Global Environmental Monitoring Unit, Institute for Environment and Sustainability, European Commission Joint Research Centre, GEM Unit, TP 272, Via E. Fermi 2749, I-21027 Ispra (VA), Italy.

M. Jung, G. Lasslop, and M. Reichstein, Model Data Integration Group, Max Planck Institute for Biogeochemistry, D-07745 Jena, Germany.

G. Kiely, HYDROMET, Civil and Environmental Engineering Department, University College Cork, College Road, Cork, Ireland.

W. Kutsch, Institut für Agrarrelevante Klimaforschung, Johann Heinrich von Thünen-Institut, D-38116 Braunschweig, Germany.

B. E. Law, Department of Forest Ecosystems and Society, Oregon State University, Corvallis, OR 97331, USA.

H. A. Margolis, Centre d'Étude de la Forêt, Faculté de Foresterie, de Géographie et de Géomatique, Université Laval, Québec, QC G1V 0A6, Canada.

L. Merbold, Grassland Science Group, Institute of Plant-, Animal- and Agroecosystem Sciences, ETH Zurich, CH-8092 Zurich, Switzerland.

L. Montagnani, Forest Services and Agency for the Environment, Autonomous Province of Bolzano, Piazza Universita' 1, I-39100 Bolzano, Italy.

E. J. Moors, Earth System Science, Climate Change, Alterra Wageningen UR, Wageningen University, PO Box 47, NL-6700 AA Wageningen, Netherlands.

D. Papale, Department of Forest Environment and Resources, University of Tuscia, via C. de Lellis, I-01100 Viterbo, Italy.

A. D. Richardson, Department of Organismic and Evolutionary Biology, Harvard University, HUH, 22 Divinity Ave., Cambridge MA 02138, USA.

F. Vaccari, Institute of Biometeorology, National Research Council, I-50144 Firenze, Italy.

C. Williams, Graduate School of Geography, Clark University, Worcester, 950 Main St., Worcester, MA 01610, USA.